Available online at www.sciencedirect.com

ScienceDirect

Current Opinion in Electrochemistry

Review Article

Oxygen desorption – Critical step for the oxygen evolution reaction

Tobias Binninger[1,2], Piotr M. Kowalski[1,2] and Michael H. Eikerling[1,2,3]

Abstract

The oxygen evolution reaction (OER) has been widely investigated in computational electrocatalysis. Recent studies suggest that the final oxygen desorption step could be rate-limiting, or even inhibiting, for the classical OER mechanism on the benchmark IrO_2 electrocatalyst, and a novel reaction mechanism has been proposed circumventing this bottleneck. In this review, we provide an overview of recent progress in OER electrocatalysis with a concise focus on computational studies that explicitly accounted for the elementary step of O_2 desorption. We highlight the computational and methodological intricacies that led to not considering this step as crucial by earlier OER studies. Key suggestions are provided for future studies to open new directions in OER electrocatalysis.

Addresses

[1] Theory and Computation of Energy Materials (IEK-13), Institute of Energy and Climate Research, Forschungszentrum Jülich GmbH, 52425 Jülich, Germany

[2] Jülich Aachen Research Alliance JARA Energy & Center for Simulation and Data Science (CSD), 52425 Jülich, Germany

[3] Chair of Theory and Computation of Energy Materials, Faculty of Georesources and Materials Engineering, RWTH Aachen University, Intzestrasse 5, 52072 Aachen, Germany

Corresponding author: Binninger, Tobias (t.binninger@fz-juelich.de)

Current Opinion in Electrochemistry 2023, **42**:101382

Edited by **Kai S. Exner**

This review comes from a themed issue on **Fundamental and Theoretical Electrochemistry (2024)**

For a complete overview see the Issue and the Editorial

Available online 1 September 2023

https://doi.org/10.1016/j.coelec.2023.101382

Keywords

Computational electrocatalysis, Oxygen evolution reaction, Oxygen desorption, Kinetics, Activation free energy.

Introduction

The oxygen evolution reaction (OER) is the ubiquitous anodic half-cell reaction of aqueous electrolysis processes for electrochemical energy conversion, such as hydrogen production and electrochemical carbon dioxide reduction. The significant overpotential of the OER substantially contributes to the overall energy loss. Decreasing the OER overpotential with the help of advanced electrocatalyst materials is therefore considered a promising route for improving the energy efficiency of such processes. Over the past two decades, computational studies based on density functional theory (DFT) have increasingly contributed to research in OER electrocatalysis [1–11].

An expedient and prolific computational procedure has been established in seminal works by Rossmeisl et al. on the OER mechanism on metal and metal-oxide electrocatalysts [1,2]. The reaction mechanism was assumed to be the mechanism of the oxygen reduction reaction in reverse, proceeding *via* surface-adsorbed intermediate oxygen-containing species *OH, *O, and *OOH,

$$M^* + H_2O \rightarrow M^*OH + H^+ + e^- \quad (1)$$

$$M^*OH \rightarrow M^*O + H^+ + e^- \quad (2)$$

$$M^*O + H_2O \rightarrow M^*OOH + H^+ + e^- \quad (3)$$

$$M^*OOH \rightarrow M^* + O_2 + H^+ + e^- \quad (4)$$

where M* denotes a free adsorption site at the catalyst surface. From DFT-computed data (energies and vibrational frequencies) of the respective reactant and product states, reaction Gibbs energy changes ΔG_i for each of the reaction steps are obtained, using the computational hydrogen electrode approach to account for free-energy contributions of electron–proton pairs [12]. The reaction step with the largest ΔG_i is commonly referred to as the potential-determining step (PDS), which is the last step to become downhill in free energy as the applied potential is increased in the range $E > \Delta G_i/e$. The "thermodynamic" overpotential, $\eta_{th} = \Delta G_{PDS}/e - 1.23\ V_{RHE}$, is a pertinent descriptor to rationalize experimentally observed activity trends across a variety of electrocatalyst materials [3]. One of the reasons for the popularity of η_{th} is that it is readily computable, whereas the real overpotential is kinetic in nature and requires the cumbersome computation of transition states and related energy barriers in combination

with a microkinetic modeling framework [5,6]. For many OER electrocatalysts, step (3), i.e., the formation of *OOH, has been identified as the PDS, *e.g.*, on iridium oxide [2] or nickel oxyhydroxide [11], although recent theoretical analysis rather suggested step (4) to be rate-determining at high overpotentials on IrO_2 [13].

The mechanism (1)−(4) is often referred to as the adsorbate evolving mechanism (AEM) and most commonly considered in theoretical studies of the OER. Alternative mechanisms with participation of lattice oxygen anions have been proposed, *e.g.*, by Binninger et al. [14] and Rong et al. [4] to explain the experimentally observed coupling between OER activity and corrosion of metal-oxide catalysts [15,16], or the appearance of isotopically labeled oxygen atoms from the oxide lattice in the evolved O_2 gas [17,18]. Nevertheless, the scheme (1)−(4) represents the "classical" benchmark mechanism, and it is assumed to proceed on standard catalysts, such as iridium dioxide [2,5,6]. However, Binninger and Doublet recently found that the OER on IrO_2 likely follows a different pathway *via* association of two neighboring *OO species [10], as shown in Figure 1,

$$Ir^{*}OO + OO^{*}Ir \xrightarrow{Ir^{*}OOOO^{*}Ir} Ir^{*}O + O_2 + O^{*}Ir \quad (5)$$

Given that iridium dioxide is the benchmark OER catalyst, both for experimental and computational studies, a major overhaul in our understanding of the relevant mechanism would be remarkable. These findings have been corroborated by Exner [19], who used the descriptor $G_{max}(\eta)$ [20], *i.e.*, the maximum free energy to be overcome along the OER pathway, for a comparative analysis of activity volcanos for the classical and novel mechanisms. Exner concluded "that the *OO·OO* recombination mechanism is of relevance for the heuristic discovery of OER materials, and thus, should not be neglected in future screening studies that make use of the concept of volcano plots."

In the present review, we analyze common gaps in computational studies that could explain why the *OO·OO* association mechanism has been overlooked before. This opens new directions for future computational investigations of OER electrocatalyst materials. Our discussion is focused on the oxygen desorption step.

Figure 1

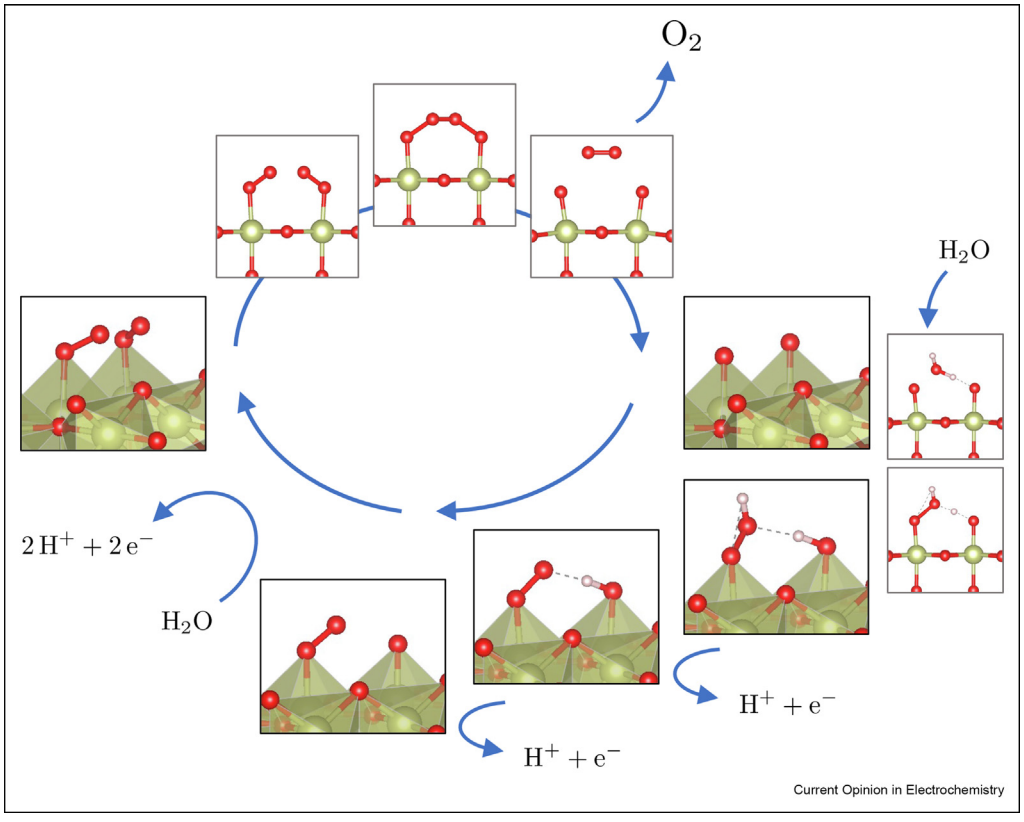

Oxygen evolution reaction pathway on IrO_2 (110) according to Binninger and Doublet [10]. The O_2 molecule is formed *via* association of two neighboring *OO species, thereby avoiding the conventional desorption step.

Other pertinent questions include the influence of the solvent and the use of explicit vs. implicit solvation models. Gauthier et al. [21] found that explicit water layers stabilize certain OER intermediates on IrO_2, especially *OOH, which form hydrogen bonds with adjacent water molecules. For oxygen desorption, however, the *OO initial state does not form hydrogen bonds, and likewise, the nonpolar O_2 molecule interacts very weakly with water molecules [5]. Questions of solvation models are thus of minor relevance for the oxygen desorption step.

Oxygen desorption: computational pitfalls

Common pitfalls for computational studies of the OER mechanism are associated with the treatment of oxygen desorption. This can make the (final) oxygen desorption step appear much more feasible than it actually is, which can result in erroneous conclusions regarding the rate-limiting step. This is analyzed in detail here.

Treatment of elementary chemical steps

Most computational studies do not consider the oxygen desorption step independently [2]. Instead, it is lumped together with the preceding deprotonation of *OOH, as shown in Equation (4). The underlying rationale of this approach is that the critical rate-limiting steps along an *electro*catalytic pathway must involve charge transfer, i.e., electron–proton transfer for the case of the OER, because only such *electrochemical* steps would lead to the experimentally observed dependence of OER kinetic currents on the applied electrode potential [2]. While this rationale has been widely adopted in computational electrocatalysis, it neglects a critical aspect. For instance, considering the chemical step of (molecular) oxygen desorption from an electrocatalyst surface, $M^*OO \rightarrow M^* + O_2$, the rate of this step is given by $r_d = \theta_{OO}\, k_d$. For a purely chemical step, *i.e.*, in absence of charge transfer/redistribution across the electrochemical double layer, the rate constant k_d will be independent of the applied potential. However, the surface coverage θ_{OO} can be strongly potential-controlled under OER conditions. Based on early works by Parsons [23], Exner and Over [22] have developed a comprehensive, albeit intuitive scheme to describe the potential dependence of intermediates and transition states along a general electrocatalytic pathway, as shown in Figure 2; at a given electrode potential, the starting point of the electrocatalytic cycle is chosen at the reaction intermediate with the lowest free energy, corresponding to the dominant surface coverage. Every subsequent intermediate's free energy is lowered by $-ne\eta$ with increasing (over)potential η, where n is the number of electron–proton transfer steps required to produce the respective intermediate from the (lowest-energy) starting point. Lowering the intermediate's free energy increases the respective surface coverage, which, in turn, increases the rate of the subsequent step. Even "chemical" steps can thus be strongly potential dependent *via* the surface coverage term in the rate equation, as long as the respective coverage is significantly smaller than one.

Figure 2

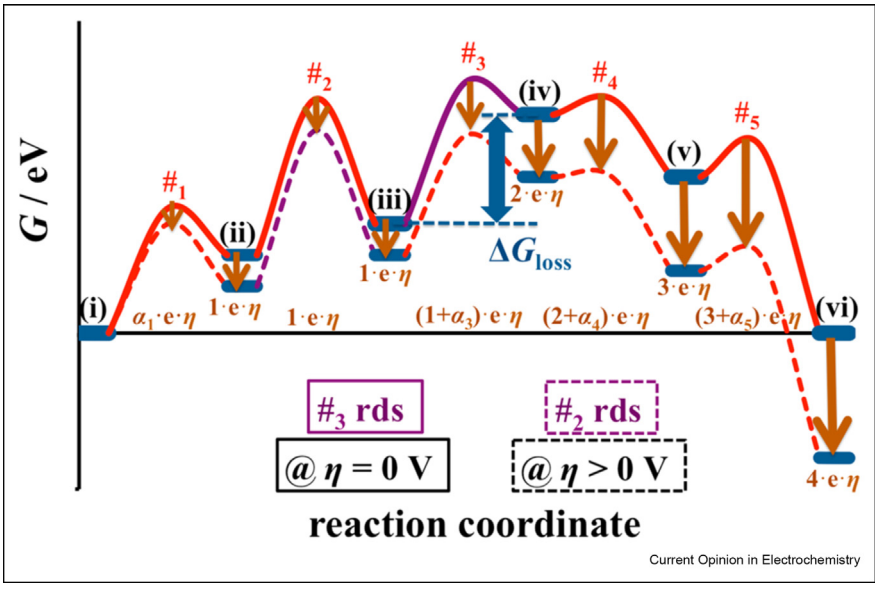

Free energy diagram of a general electrocatalytic process involving one chemical (ii → iii) and four electrochemical steps. The chemical step is sensitive to the applied potential *via* the free energy/coverage of the corresponding reactant intermediate (ii). Reprinted (adapted) with permission from K.S. Exner and H. Over [22], *Acc. Chem. Res.* 2017, 50, 5, 1240–1247. Copyright 2017 American Chemical Society.

A similar picture emerges naturally if formal consideration to all intermediates is given in a full microkinetic multistep treatment, leading to the concept of the rate-determining term (RDT) recently proposed by Huang et al. [24] This approach generalizes the simplified concepts of the PDS and rate-determining step without requiring the existence of a single critical step. Both chemical and electrochemical steps are treated on an equal footing, and the dependencies of activation barriers (rate constants) and coverage terms on the applied electrode potential are consistently accounted for in the rate expressions for each step. Each elementary step contributes toward the overall reaction rate and must be included in this approach.

Elementary *chemical* steps, therefore, cannot be excluded *a priori* from the set of relevant steps to be considered for *electrocatalytic* multistep reactions. For the OER, Ping et al. [5] included chemical steps in their computational study of the OER mechanism on IrO_2, which made an important contribution toward a more detailed understanding of the OER mechanism. In their approach, step (4) was split into an elementary deprotonation step,

$$M^*OOH \rightarrow M^*OO + H^+ + e^- \quad (6)$$

and a subsequent desorption step,

$$M^*OO \rightarrow M^* + O_2 \quad (7)$$

The separate treatment of both elementary steps can strongly alter the picture of the free-energy profile along the OER pathway. On IrO_2 (110), *e.g.*, the *OOH deprotonation step (6) is exergonic with $\Delta G_{OOH \rightarrow OO+H^+ + e^-} = -0.27\,eV$ (at the OER reversible potential of $1.23\,V_{RHE}$), whereas the subsequent O_2 desorption step (7) is strongly endergonic with $\Delta G_{OO \rightarrow {}^* + O_2} = +0.53\,eV$ [10]. We note that this value holds regardless of whether the oxygen molecule is considered in the gas phase or is dissolved in water, as long as saturation is assumed under the same partial pressure. In contrast, following the conventional approach of lumping both steps into one, *cf.* Equation (4), a much weaker endergonic change in free energy is obtained as the sum of both elementary contributions, $\Delta G_{OOH \rightarrow {}^* + O_2 + H^+ + e^-} = +0.26\,eV$, which misleadingly makes the combined step appear very feasible.

Several computational studies have lumped the O_2 desorption step together with the subsequent adsorption of H_2O or OH^- at the same surface cation site [4,9]. This approach can mask the actual barrier of oxygen desorption by avoiding the possibly unfavorable undercoordinated state of the surface metal cation. For the case of IrO_2, in particular, the unfavorable energetics of the unsaturated Ir* has been identified as the main reason for the high oxygen desorption barrier [10]. Importantly, Ping et al. [5] performed a nudged-elastic band (NEB) calculation considering the possibility of simultaneous O_2 desorption and H_2O adsorption (see Figure 3). However, the authors found that both steps proceed sequentially and must therefore be considered independently.

Activation barrier *vs.* free energy of oxygen desorption

Another pitfall lies in the treatment of free-energy contributions for the oxygen desorption step. Typically, the activation barriers of the OER pathway are not explicitly calculated, which are generally cumbersome to determine, *e.g.*, by the NEB method [5,10,25] or more expensive methods such as *ab initio* metadynamics [26]. Instead, most computational studies are restricted to the calculation of reaction intermediates' free energies, from which the PDS is obtained as described earlier. As explained by Razzaq et al. [20], this approach is motivated by the Brønsted–Evans–Polanyi (BEP) principle according to which there exists an approximate linear relationship between activation energy (from reactant to transition state) and reaction energy (from reactant to product state) within a series of "similar" reactions [27–29]. It must, however, be emphasized that the BEP principle has been established for the relationship between the activation energy and the reaction *enthalpy* ΔH_i [30,31]. As long as entropy contributions are of similar magnitude, the BEP relationship also holds when using reaction *Gibbs energies*, $\Delta G_i = \Delta H_i - T\Delta S_i$, instead of enthalpy. Similar entropy contributions could be expected for surface-adsorbed intermediates, so this approach appears well justified for steps (1)–(3). However, this does not hold for step (4) (or step (7)) involving oxygen desorption, where entropies are very different between reactants and products at the respective standard states. Besides vibrational (and solvation) entropy contributions, the surface-adsorbed reactant M*OO comprises configurational entropy due to the (random) distribution across available surface sites. The latter can be estimated from

Figure 3

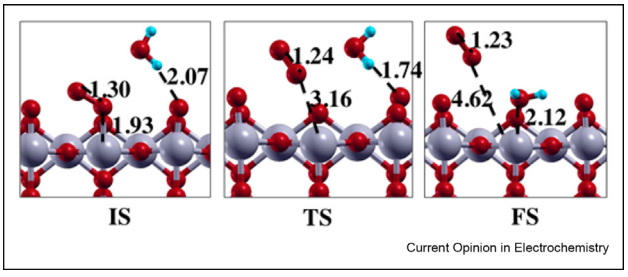

Nudged-elastic band calculation of oxygen desorption and subsequent water adsorption. Reprinted (adapted) with permission from Ping et al. [5], *J. Am. Chem. Soc.* 2017, 139, 1, 149–155. Copyright 2016 American Chemical Society.

the ideal entropy of mixing, yielding a contribution of $-T\frac{\partial}{\partial\theta}S^{\mathrm{conf}}_{*\mathrm{OO}} = k_{\mathrm{B}}T\log\left(\frac{\theta}{1-\theta}\right)$ to the respective chemical potential, which is zero at the standard-state coverage of $\theta = 1/2$ [32]. In contrast, besides vibrational–rotational contributions, the final state of the *free* O_2 molecule comprises entropy due to translational degrees of freedom. From the Sackur-Tetrode expression for ideal-gas entropy, the latter is estimated as $-TS^{\mathrm{trans}}_{\mathrm{O_2}} \approx -0.47\,\mathrm{eV}$ under standard conditions ($p_{\mathrm{O_2}} = 1$ bar and $T = 298.15$ K). Thus, the majority of the total entropy contribution of $-TS^{\ominus}_{\mathrm{O_2}} = -0.63\,\mathrm{eV}$ to the free energy of gaseous oxygen [33] originates from translational degrees of freedom. The corresponding drastic change in entropy between initial and final state thwarts the applicability of the BEP principle when comparing step (4) with the other steps (1)–(3). This critical point is neglected in common computational approaches. As a crude correction, one could simply remove the translational entropy contribution by adding +0.47 eV to the free energy of oxygen gas. Applying this correction to the Gibbs energy change of the final desorption step on IrO_2 (110) ($\Delta G_{\mathrm{OO}\rightarrow{}^*+\mathrm{O_2}} = +0.53\,\mathrm{eV}$, mentioned earlier), we obtain $\Delta G^{\mathrm{w/o\ trans}}_{\mathrm{OO}\rightarrow{}^*+\mathrm{O_2}} = 1.00\,\mathrm{eV}$ without translational entropy in the final state (w/o trans). This estimation indicates a significant uphill energy cost of approx. 1.00 eV, suggesting that oxygen desorption could be rate-limiting for the classical mechanism on IrO_2. We note that this value would not be altered to any significant extent when accounting for solvation effects. This can be estimated based on the enthalpy of solution of oxygen in water, which is $-12\ \mathrm{kJ\ mol^{-1}}$ at room temperature [34], or −0.12 eV per oxygen molecule.

A. closer look at the activation barrier for oxygen desorption

Ping et al. [5] directly computed the activation energy barrier for O_2 desorption from the IrO_2 (110) surface using the climbing-image NEB method. To estimate the corresponding *free* energy of activation, they added entropic contributions of final-state O_2 to the DFT energy at the transition state. This approach, however, is inconsistent. As discussed earlier, the entropy of the final-state O_2 is dominated by the translational degrees of freedom, which the transition state does *not* possess. The translational free-energy contribution is strongly dependent on the product gas concentration, or partial pressure, *via* the typical expression $k_{\mathrm{B}}T\log(p_{\mathrm{O_2}})$. Erroneously adding such contribution to the free energy of activation, $\Delta^{\ddagger}G$, would yield an oxygen desorption rate $r_{\mathrm{d}} \propto \exp(-\Delta^{\ddagger}G/k_{\mathrm{B}}T) \propto p_{\mathrm{O_2}}^{-1}$, *i.e.*, inversely proportional to the product gas partial pressure. This contradicts the basic principle that the forward rate of an elementary step only depends on the reactant concentration and is independent from the product concentration.

Another DFT study of the OER mechanism explicitly accounting for the chemical oxygen desorption step (7) was presented by Dickens et al. [6]. They applied microkinetic modeling with DFT-computed parameters, *i.e.*, equilibrium constants and activation energies, to include both thermodynamic and kinetic aspects in the analysis of scaling relations and activity trends between the rutile-type oxides RuO_2, IrO_2, RhO_2, and PtO_2. To avoid well-known deficiencies of DFT in the description of the O_2 molecule [35,36], the activation energy of the oxygen desorption step was *not* determined from the NEB method. Instead, Dickens et al. first estimated an activation free-energy barrier of 0.28 eV for O_2 desorption from RuO_2 (110), based on experimental thermal desorption spectra published by Kim et al. [37] Then, a linear BEP relationship with unity slope between the O_2 desorption barrier and (DFT-computed) binding energy was assumed to estimate the corresponding values for other oxides. For IrO_2 (110), in particular, a value of 0.98 eV was obtained. However, the authors finally rejected this value because it led to the conclusion that the O_2 desorption step was rate-determining, which they considered inconsistent with experimental observations regarding the maximum possible current magnitude and potential dependence.

Binninger and Doublet [10] directly calculated the energy barrier for O_2 desorption from the IrO_2 (110) surface using the climbing image NEB method. Interestingly, they obtained an activation energy of 0.95 eV, see Figure 4a, which is very close to the value estimated by Dickens et al. [6]. Moreover, this value is very close to the value of 1.00 eV estimated earlier by correcting the translational entropy contribution for the final state. Thus, there exists strong evidence that the desorption step (7) is rate-limiting, or even inhibiting, for the classical OER mechanism on IrO_2. This becomes directly apparent when considering the ensemble of all steps in the free-energy diagram in Figure 4c, reproduced from Binninger and Doublet [10]. The O_2 desorption step not only has the highest individual barrier, but the respective barrier top also marks the highest point along the free-energy profile to be overcome for the standard OER pathway. The apparent inconsistency with the excellent OER activity of IrO_2, which had prevented Dickens et al. [6] from drawing the same conclusion, is resolved by the novel mechanism proposed by Binninger and Doublet [10] in providing a bypass for the inhibitive classical desorption step, see Figure 4b,c.

Electrochemical experiments are typically performed under potentiostatic conditions. This corresponds to a grand canonical (GC) setting for DFT simulations [38,39]. Grand canonical–DFT methods, however, are significantly more complicated and are less available than standard DFT methods at a constant electron number. As a viable alternative, calculations can

Figure 4

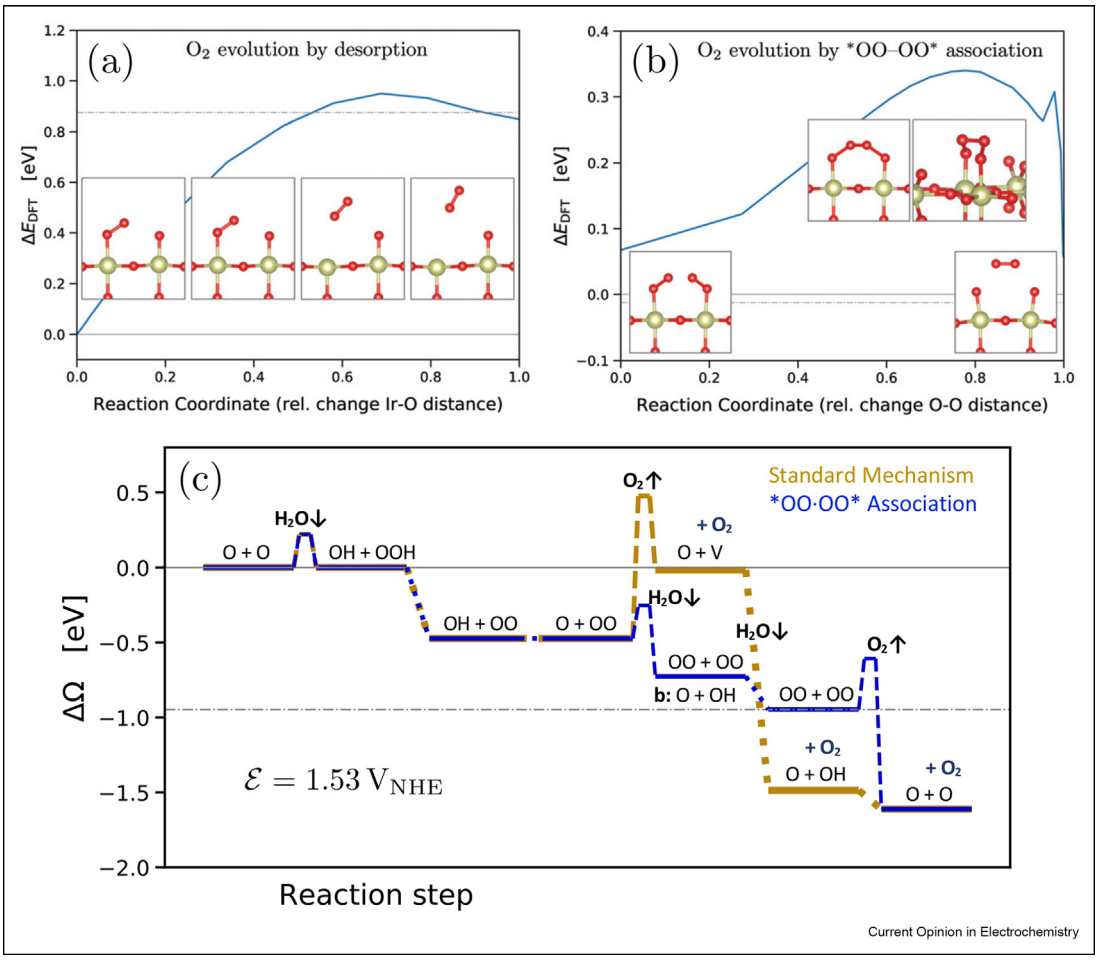

Computed energy barriers for O_2 desorption **(a)** and *OO ·OO* association **(b)** from nudged-elastic band calculations for IrO_2 (110); **(c)** free-energy diagram of the conventional *vs.* *OO ·OO* association mechanisms of the oxygen evolution reaction on IrO_2 (110) at an applied electrode potential of $\mathcal{E} = 1.53\,V_{NHE}$. Reprinted (adapted) from Binninger and Doublet [10], *Energy Environ. Sci.* 2022, 15, 2519–2528. CC BY-NC 3.0.

be performed at various (fixed) electron numbers, and the corresponding results can be extrapolated/interpolated to the target applied potential [40—42]. Although oxygen desorption is of chemical nature, the difference in initial vs. final state of the electrocatalyst surface can alter the surface dipole and shift the corresponding potential of zero charge. The question of constant charge vs. constant potential calculations thus remains relevant also for such "chemical" steps.

DFT errors around the oxygen desorption step

Besides the outlined problems with accounting for the entropy of molecular oxygen, the computational treatment of oxygen desorption is complicated by significant deficiencies inherent to DFT under the commonly used generalized gradient approximation (GGA). The already mentioned problem with the computation of the O_2 molecule results in a significant overestimation of the O_2 binding energy [35], introducing an error of about 0.4 eV in the computed free energy of the water splitting reaction [10,36]. Whereas the free energy of gaseous O_2 in the final state can be corrected *via* a thermodynamic cycle and usage of experimental reference values [35], *e.g.*, for the free energy of water splitting [36], it remains unclear to what extent similar errors affect the DFT energies of surface-adsorbed *OO and how such errors evolve along the desorption path [6]. However, the DFT error is expected to be smaller for adsorbed species with a superoxide ($^*OO^-$) character [5,9]. Accordingly, correction of such DFT errors along the desorption pathway would raise the final state with respect to the initial state, thus further increasing the effective desorption barrier [10].

There is another general problem with DFT when computing transition metal elements. These show strong *d*-electron correlations due to the presence of Coulomb on-site interactions, as indicated by significant

values of the Hubbard U parameters [43,44]. Transition metal compounds with a band gap (*e.g.*, TiO_2) [45] are therefore commonly treated by the DFT + U method. In contrast, transition metal oxides with a metallic character (*e.g.*, IrO_2 or RuO_2) [46] are usually successfully modeled with a standard GGA-DFT approach [47–49]. Thus, different computational schemes are proposed for compounds with and without a band gap, making it difficult to model mixed compounds, *e.g.*, TiO_2–RuO_2 solid solutions [44,50]. Moreover, the corresponding errors of each method can be substantially different for surface transition metal cations in the fully coordinated initial *vs.* the coordinately unsaturated final state of the O_2 desorption step. It is therefore important to evaluate systematically the accuracy of different levels of DFT, including GGA, GGA + U, and hybrid functionals. Gono and Pasquarello [51] found significant differences between GGA vs. hybrid functionals in the computed free-energy steps of the OER on a variety of catalysts. Although hybrid functionals are often considered more accurate, for compounds containing transition metal elements, they often overestimate band gaps and hydrogen-binding energies [52,53]. The comparison between results of semilocal vs. hybrid functionals is recommended to estimate the uncertainty in the computed free energies [51].

Conclusion and outlook

The oxygen desorption step has been inconsistently treated in most computational studies of the OER mechanism on various electrocatalyst materials. Carefully accounting for this step will be relevant in future studies to understand under which circumstances the respective energy barrier becomes inhibitive for the classical mechanism. This could help to identify electrocatalyst materials with similar properties as those of IrO_2 in terms of combined stability and OER activity. To this end, we arrive at the following recommendations.

- The oxygen desorption step should be treated as an elementary step, separate from preceding deprotonation or subsequent H_2O or OH^- adsorption steps.
- It must be carefully considered which entropic contributions to include in the free-energy barrier of the desorption step. In particular, biasing the apparent barrier due to translational final-state contributions must be avoided.
- For accurate predictions, DFT-based methods must be used with caution when computing molecular oxygen as well as changes in the redox state of transition-metal cations. Conclusions derived thereof should be tested for robustness under realistically estimated errors.
- The influence of oxygen desorption barriers on the overall reaction kinetics should be evaluated within a microkinetic modeling framework accounting for the ensemble of all steps and the mutual dependencies of intermediates' coverages due to competition for available adsorption sites.

We wish to point out that we exemplified these issues mostly for the AEM. However, our discussion equally applies to so-called lattice oxygen mechanisms, where the essential step of oxygen evolution is accompanied by the formation of an oxygen vacancy in the surface layer of the oxide lattice. Ultimately, computational results must be evaluated by comparison with data from thermal desorption experiments, as presented, *e.g.*, by Kim et al. [37] for RuO_2 and Martin et al. [54] and Abb et al. [55] for IrO_2. Vice versa, the assignment of experimentally observed desorption peaks requires computational support to distinguish between competing mechanisms, such as classical desorption ($M^*OO \rightarrow M^* + O_2$) vs. associative desorption, i.e., $2\ M^*OO \rightarrow 2\ M^*O + O_2$ or $2\ M^*O \rightarrow 2\ M^* + O_2$.

Declaration of competing interest

The authors declare that they have no known competing financial interests or personal relationships that could have appeared to influence the work reported in this paper.

Data availability

No data was used for the research described in the article.

Acknowledgements

The presented work was carried out within the framework of the Helmholtz Association's program Materials and Technologies for the Energy Transition under the topic Chemical Energy Carriers and the subtopic Electrochemistry for Hydrogen.

References

Papers of particular interest, published within the period of review, have been highlighted as:

** of outstanding interest

1. Rossmeisl J, Logadottir A, Nørskov JK: **Electrolysis of water on (oxidized) metal surfaces**. *Chem Phys* 2005, **319**:178–184.

2. Rossmeisl J, Qu ZW, Zhu H, Kroes GJ, Nørskov JK: **Electrolysis of water on oxide surfaces**. *J Electroanal Chem* 2007, **607**: 83–89.

3. Man IC, Su H-Y, Calle-Vallejo F, Hansen HA, Martínez JI, Inoglu NG, Kitchin J, Jaramillo TF, Nørskov JK, Rossmeisl J: **Universality in oxygen evolution electrocatalysis on oxide surfaces**. *ChemCatChem* 2011, **3**:1159–1165.

4. Rong X, Parolin J, Kolpak AM: **A fundamental relationship between reaction mechanism and stability in metal oxide catalysts for oxygen evolution**. *ACS Catal* 2016, **6**:1153–1158.

5. ** Ping Y, Nielsen RJ, Goddard III WA: **The reaction mechanism with free energy barriers at constant potentials for the oxygen evolution reaction at the IrO_2 (110) surface**. *J Am Chem Soc* 2017, **139**:149–155.

As part of this DFT study, it was demonstrated that oxygen desorption must be considered as an own elementary step of the OER pathway on IrO_2, independent from preceding deprotonation or subsequent adsorption processes.

6. ** Dickens CF, Kirk C, Nørskov JK: **Insights into the electrochemical oxygen evolution reaction with ab initio calculations and microkinetic modeling: beyond the limiting potential volcano**. *J Phys Chem C* 2019, **123**:18960–18977.
Computational study of the OER combining DFT and microkinetic modeling. For the first time, it was acknowledged that presently available data, both computational and experimental, indicate a dominating energy barrier for oxygen desorption on IrO_2. However, the physical significance of this result was not discussed.

7. Buvat G, Eslamibidgoli MJ, Youssef AH, Garbarino S, Ruediger A, Eikerling M, Guay D: **Effect of IrO_6 octahedron distortion on the OER activity at (100) IrO_2 thin film**. *ACS Catal* 2020, **10**: 806–817.

8. Nong HN, Falling LJ, Bergmann A, Klingenhof M, Tran HP, Spöri C, Mom R, Timoshenko J, Zichittella G, Knop-Gericke A, Piccinin S, Pérez-Ramírez J, Cuenya BR, Schlögl R, Strasser P, Teschner D, Jones TE: **Key role of chemistry versus bias in electrocatalytic oxygen evolution**. *Nature* 2020, **587**:408–413.

9. González D, Heras-Domingo J, Sodupe M, Rodríguez-Santiago L, Solans-Monfort X: **Importance of the oxyl character on the IrO_2 surface dependent catalytic activity for the oxygen evolution reaction**. *J Catal* 2021, **396**:192–201.

10. ** Binninger T, Doublet M-L: **The Ir–OOOO–Ir transition state and the mechanism of the oxygen evolution reaction on IrO_2(110)**. *Energy Environ Sci* 2022, **15**:2519–2528.
First DFT study to identify oxygen desorption as rate-inhibiting for the classical OER mechnanism on IrO_2. A novel *OO •OO* association mechanism has been proposed to bypass the critical desorption step.

11. ** He Z-D, Tesch R, Eslamibidgoli MJ, Eikerling MH, Kowalski PM: **Low-spin state of Fe in Fe-doped NiOOH electrocatalysts**. *Nat Commun* 2023, **14**:3498.
This study showed that carefully accounting for *d*-electron correlation with a refined DFT + U method is highly relevant for correctly predicting the electrocatalytic properties of certain transition metal oxides toward OER.

12. Nørskov JK, Rossmeisl J, Logadottir A, Lindqvist L, Kitchin JR, Bligaard T, Jónsson H: **Origin of the overpotential for oxygen reduction at a fuel-cell cathode**. *J Phys Chem B* 2004, **108**: 17886–17892.

13. Exner KS, Over H: **Beyond the rate-determining step in the oxygen evolution reaction over a single-crystalline IrO2(110) model electrode: kinetic scaling relations**. *ACS Catal* 2019, **9**: 6755–6765.

14. Binninger T, Mohamed R, Waltar K, Fabbri E, Levecque P, Kötz R, Schmidt TJ: **Thermodynamic explanation of the universal correlation between oxygen evolution activity and corrosion of oxide catalysts**. *Sci Rep* 2015, **5**, 12167.

15. Danilovic N, Subbaraman R, Chang K-C, Chang SH, Kang YJ, Snyder J, Paulikas AP, Strmcnik D, Kim Y-T, Myers D, Stamenkovic VR, Markovic NM: **Activity–stability trends for the oxygen evolution reaction on monometallic oxides in acidic environments**. *J Phys Chem Lett* 2014, **5**:2474–2478.

16. Cherevko S, Reier T, Zeradjanin AR, Pawolek Z, Strasser P, Mayrhofer KJJ: **Stability of nanostructured iridium oxide electrocatalysts during oxygen evolution reaction in acidic environment**. *Electrochem Commun* 2014, **48**:81–85.

17. Wohlfahrt-Mehrens M, Heitbaum J: **Oxygen evolution on Ru and RuO_2 electrodes studied using isotope labelling and on-line mass spectrometry**. *J Electroanal Chem Interfacial Electrochem* 1987, **237**:251–260.

18. Fierro S, Nagel T, Baltruschat H, Comninellis C: **Investigation of the oxygen evolution reaction on Ti/IrO_2 electrodes using isotope labelling and on-line mass spectrometry**. *Electrochem Commun* 2007, **9**:1969–1974.

19. ** Exner KS: **Implications of the M-OO ‥OO-M recombination mechanism on materials screening and the oxygen evolution reaction**. *JPhys Energy* 2022, **5**, 014008.
Comparative analysis of activity volcanos for classical and *OO •OO* association mechanisms, demonstrating that both mechanisms must be considered for OER electrocatalyst screening.

20. Razzaq S, Exner KS: **Materials screening by the descriptor gmax(η): the free-energy span model in electrocatalysis**. *ACS Catal* 2023, **13**:1740–1758.

21. Gauthier JA, Dickens CF, Chen LD, Doyle AD, Nørskov JK: **Solvation effects for oxygen evolution reaction catalysis on IrO2(110)**. *J Phys Chem C* 2017, **121**:11455–11463.

22. Exner KS, Over H: **Kinetics of electrocatalytic reactions from first-principles: a critical comparison with the ab initio thermodynamics approach**. *Acc Chem Res* 2017, **50**:1240–1247.

23. Parsons R: **General equations for the kinetics of electrode processes**. *Trans Faraday Soc* 1951, **47**:1332–1344.

24. ** Huang J, Zhu X, Eikerling M: **The rate-determining term of electrocatalytic reactions with first-order kinetics**. *Electrochim Acta* 2021, **393**:139019.
Theoretical treatment of electrocatalytic multistep reactions leading to the concept of the rate-determining term. Both chemical and electrochemical steps are consistently accounted for overcoming simplifications inherent to the common concepts of PDS and rate-determining step.

25. Henkelman G, Uberuaga BP, Jónsson H: **A climbing image nudged elastic band method for finding saddle points and minimum energy paths**. *J Chem Phys* 2000, **113**:9901–9904.

26. Yang X, Bhowmik A, Vegge T, Anton Hansen H: **Neural network potentials for accelerated metadynamics of oxygen reduction kinetics at Au–water interfaces**. *Chem Sci* 2023, **14**: 3913–3922.

27. Bronsted JN: **Acid and basic catalysis**. *Chem Rev* 1928, **5**: 231–338.

28. Evans MG, Polanyi M: **Inertia and driving force of chemical reactions**. *Trans Faraday Soc* 1938, **34**:11–24.

29. Nørskov JK, Bligaard T, Logadottir A, Bahn S, Hansen LB, Bollinger M, Bengaard H, Hammer B, Sljivancanin Z, Mavrikakis M, Xu Y, Dahl S, Jacobsen CJH: **Universality in heterogeneous catalysis**. *J Catal* 2002, **209**:275–278.

30. Bligaard T, Nørskov JK, Dahl S, Matthiesen J, Christensen CH, Sehested J: **The brønsted–evans–polanyi relation and the volcano curve in heterogeneous catalysis**. *J Catal* 2004, **224**: 206–217.

31. Cheng J, Hu P, Ellis P, French S, Kelly G, Lok CM: **Brønsted-evans-polanyi relation of multistep reactions and volcano curve in heterogeneous catalysis**. *J Phys Chem C* 2008, **112**: 1308–1311.

32. Parsons R: **The rate of electrolytic hydrogen evolution and the heat of adsorption of hydrogen**. *Trans Faraday Soc* 1958, **54**: 1053–1063.

33. Cox JD, Wagman DD, Medvedev VA: *CODATA key values for thermodynamics*. New York: Hemisphere Publishing Corp.; 1989.

34. Gill SJ, Wadsö I: **Flow-microcalorimetric techniques for solution of slightly soluble gases. Enthalpy of solution of oxygen in water at 298.15 K**. *J Chem Therm* 1982, **14**:905–919.

35. Kowalski PM, Meyer B, Marx D: **Composition, structure, and stability of the rutile TiO_2(110) surface: oxygen depletion, hydroxylation, hydrogen migration, and water adsorption**. *Phys Rev B* 2009, **79**, 115410.

36. Sargeant E, Illas F, Rodríguez P, Calle-Vallejo F: **Importance of the gas-phase error correction for O_2 when using DFT to model the oxygen reduction and evolution reactions**. *J Electroanal Chem* 2021, **896**, 115178.

37. Kim YD, Seitsonen AP, Wendt S, Wang J, Fan C, Jacobi K, Over H, Ertl G: **Characterization of various oxygen species on an oxide surface: RuO_2(110)**. *J Phys Chem B* 2001, **105**: 3752–3758.

38. Sundararaman R, Goddard III WA, Arias TA: **Grand canonical electronic density-functional theory: algorithms and applications to Electrochemistry**. *J Chem Phys* 2017, **146**, 114104.

39. Melander MM, Kuisma MJ, Christensen TEK, Honkala K: **Grand-canonical approach to density functional theory of electro-catalytic systems: thermodynamics of solid-liquid interfaces at constant ion and electrode potentials**. *J Chem Phys* 2018, **150**, 041706.

40. Hörmann NG, Marzari N, Reuter K: **Electrosorption at metal surfaces from first principles**. *npj Comput Mater* 2020, **6**:1–10.

41. Hagopian A, Doublet M-L, Filhol J-S, Binninger T: **Advancement of the homogeneous background method for the computational simulation of electrochemical interfaces**. *J Chem Theor Comput* 2022, **18**:1883–1893.

42. Abidi N, Steinmann SN: **How are transition states modeled in heterogeneous electrocatalysis?** *Curr Opin Electrochem* 2022, **33**, 100940.

43. Şaşıoğlu E, Friedrich C, Blügel S: **Effective Coulomb interaction in transition metals from constrained random-phase approximation**. *Phys Rev B* 2011, **83**, 121101.

44. Tesch R, Kowalski PM: **Hubbard *U* parameters for transition metals from first principles**. *Phys Rev B* 2022, **105**, 195153.

45. Kowalski PM, Camellone MF, Nair NN, Meyer B, Marx D: **Charge localization dynamics induced by oxygen vacancies on the TiO_2(110) surface**. *Phys Rev Lett* 2010, **105**, 146405.

46. Jain A, Hautier G, Ong SP, Moore CJ, Fischer CC, Persson KA, Ceder G: **Formation enthalpies by mixing GGA and GGA +*U* calculations**. *Phys Rev B* 2011, **84**, 045115.

47. Hofmann T, Yu TH, Folse M, Weinhardt L, Bär M, Zhang Y, Merinov BV, Myers DJ, Goddard WAI, Heske C: **Using photoelectron spectroscopy and quantum mechanics to determine d-band energies of metals for catalytic applications**. *J Phys Chem C* 2012, **116**:24016–24026.

48. Kahk JM, Poll CG, Oropeza FE, Ablett JM, Céolin D, Rueff J-P, Agrestini S, Utsumi Y, Tsuei KD, Liao YF, Borgatti F, Panaccione G, Regoutz A, Egdell RG, Morgan BJ, Scanlon DO, Payne DJ: **Understanding the electronic structure of IrO_2 using hard-X-ray photoelectron spectroscopy and density-functional theory**. *Phys Rev Lett* 2014, **112**, 117601.

49. Ping Y, Galli G, Goddard III WA: **Electronic structure of IrO_2: the role of the metal d orbitals**. *J Phys Chem C* 2015, **119**: 11570–11577.

50. Wang X, Wan X, Qin X, Chen C, Qian X, Guo Y, Xu Q, Cai W-B, Yang H, Jiang K: **Electronic structure modulation of RuO_2 by TiO_2 enriched with oxygen vacancies to boost acidic O_2 evolution**. *ACS Catal* 2022, **12**:9437–9445.

51. Gono P, Pasquarello A: **Oxygen evolution reaction: bifunctional mechanism breaking the linear scaling relationship**. *J Chem Phys* 2020, **152**, 104712.

52. Seo D-H, Urban A, Ceder G: **Calibrating transition-metal energy levels and oxygen bands in first-principles calculations: accurate prediction of redox potentials and charge transfer in lithium transition-metal oxides**. *Phys Rev B* 2015, **92**, 115118.

53. Ting Y-Y, Kowalski PM: **Refined DFT + U method for computation of layered oxide cathode materials**. *Electrochim Acta* 2023, **443**, 141912.

54. Martin R, Kim M, Lee CJ, Shariff MS, Feng F, Meyer RJ, Asthagiri A, Weaver JF: **Molecular chemisorption of N2 on IrO2(110)**. *J Chem Phys* 2020, **152**, 074712.

55. Abb MJS, Weber T, Langsdorf D, Koller V, Gericke SM, Pfaff S, Busch M, Zetterberg J, Preobrajenski A, Grönbeck H, Lundgren E, Over H: **Thermal stability of single-crystalline IrO2(110) layers: spectroscopic and adsorption studies**. *J Phys Chem C* 2020, **124**:15324–15336.